Right-hemisphere frontoparietal oscillations precede conscious reports of visual targets

Alfredo Spagna[1], Jianghao Liu[2,3], Paolo Bartolomeo[2]

[1] Department of Psychology, Columbia University in the City of New York, NY, USA, 10027

[2] Sorbonne Université, Inserm, CNRS, Paris Brain Institute, ICM, Hôpital de la Pitié-Salpêtrière, 75013 Paris, France

[3] Dassault Systèmes, Vélizy-Villacoublay, France, 78140

Abbreviated title (50 characters maximum): Right frontoparietal oscillations precede conscious reports

Corresponding author email address: as5559@columbia.edu

Number of pages: 37

Number of figures: 5

Number of tables: 0; Supplementary Tables: 1

Number of words for Abstract: 250

Number of words for Introduction: 589

Number of words for Discussion: 1500

Conflict of Interest: The authors declare that they have no competing financial interests.

Acknowledgements: We would like to thank Brigitte C. Kaufmann, Ph.D. and Monica N. Toba, Ph.D. for providing insightful comments and suggestions. The work of P.B. is supported by the Agence Nationale de la Recherche through ANR-16-CE37-0005 and ANR-10-IAIHU-06, and by the Fondation pour la Recherche sur les AVC through FR-AVC-017. The work of J.L. is supported by specific funding from INSERM and Dassault Systèmes. Author Contribution: literature search: all authors; project administration: P. B. Data Analysis: A. S. Writing - review & editing: All authors.

Abstract

What neural events precede conscious reports? Hemisphere-asymmetric frontoparietal networks are causally related to conscious perception (Bartolomeo et al., 2025; Kaufmann et al., 2024), but their spectrotemporal dynamics remain unclear. Here, we examined frontoparietal gamma oscillations occurring before a near-threshold target during the understudied pre-target period. In 67% of trials, a supra-threshold visual cue appeared near the target placeholder box (cued condition), indicating a higher probability that the target would appear at that location. In the remaining 33% of trials (uncued condition), the target appeared at the opposite location. We measured whole-brain activity using magnetoencephalography and analyzed gamma-band oscillations, coherence, and amplitude coupling with theta-phase in 16 regions of interest involved in attentional and perceptual processes (Martín-Signes et al., 2024). Results revealed that: (1) Report of cued targets was preceded by gamma-band oscillations in the right-hemisphere (RH) superior frontal gyrus, and by theta-gamma phase-amplitude coupling in the RH superior parietal region, suggesting preparatory attention. (2) Report of uncued targets was preceded by RH inferior parietal gamma oscillations and by coherence between RH superior and middle frontal regions, supporting an anticipatory "lookout" mechanism involved in monitoring for unexpected stimuli and rapidly redirecting attention to them. (3) Unreported targets were preceded by gamma-band oscillations in the left-hemisphere superior parietal lobe and by higher coherence in the left-hemisphere frontoparietal networks, suggesting a pre-target bias contributing to omission errors (Bartolomeo et al., 2025). These spectrotemporal signatures of attention in hemisphere-asymmetric frontoparietal networks shape predictive processing and perceptual bias, and predict conscious reports or their absence.

Significance statement (120/120):

The ability to attend to spatial cues in anticipation of relevant stimuli is essential for efficient behavior. We identify three spectrotemporal dynamics by which frontoparietal networks shape conscious visual perception. Gamma-band oscillations in the right-hemisphere superior frontal gyrus and theta-gamma coupling in the right superior parietal region preceded conscious reports of cued near-threshold targets. When targets appeared in the uncued location, requiring attentional reorienting, conscious report was preceded by gamma-band oscillations in the right-hemisphere intraparietal sulcus and by coherence-based communication between the right-lateralized superior and middle frontal gyri. Conversely, left-hemispheric gamma-band oscillations and coherence during the cue-target interval disrupted conscious report. These results characterize the neural dynamics leading to conscious perception by unveiling the role of hemisphere-asymmetric frontoparietal spectral dynamics.

Keywords (5/5): attention & consciousness interactions, gamma oscillations & phase-amplitude coupling, coherence, frontoparietal networks, magnetoencephalography.

Introduction

Spatial cues guide our behavior by helping identify crucial information and potential dangers. For example, blinking traffic lights signal the need for increased attention and rapid decision-making at intersections. What neural processes enable the rapid, conscious processing of an upcoming target? Frontoparietal oscillations have been proposed as a key neural mechanism supporting the conscious processing of targets after their appearance (Nobre & Van Ede, 2023; Tosoni et al., 2023). However, their role *before* target onset remains less explored, despite this being the critical period for attentional allocation (Fries, 2023). We address this gap by investigating the contribution of multiple spectrotemporal dynamics in response to predictive peripheral cues—often indicating the target position—preceding near-threshold targets.

Previous research has clarified behavioral, structural, and functional aspects of frontoparietal networks in attention and conscious perception (Martín-Signes et al., 2024; Xuan et al., 2016). Spatial attention alters perception via exogenous or endogenous mechanisms, either modifying sensory signals (Carrasco, 2011; Carrasco & Barbot, 2019; Chica et al., 2013; Hanning et al., 2019) or biasing decision criteria (Bang & Rahnev, 2017). Exogenous cues capture attention automatically, while predictive cues engage endogenous, voluntary shifts (Asanowicz et al., 2023). Peripheral predictive cues engage both processes (Chica et al., 2011, 2013; Spagna et al., 2022), and use partially overlapping frontoparietal circuits (Behrmann et al., 2004; Landry et al., 2024; Shomstein, 2012; Spagna et al., 2022; Toba et al., 2023; Tosoni et al., 2023).

The Dorsal Attention Network (DAN), including the intraparietal sulcus, superior parietal lobule, and frontal eye fields, sends top-down signals supporting conscious report (Botta et al., 2014; Chica et al., 2013; Corbetta et al., 2008; Dugué et al., 2020; Liu, et al., 2023). The Ventral

Attention Network (VAN), mainly right-lateralized, supports target detection and reorienting (Corbetta et al., 2002; Doricchi et al., 2010; Liu, et al., 2023). These networks are connected by the three branches of the superior longitudinal fasciculus (Thiebaut De Schotten et al., 2005, 2011). The superior branch (SLF I) connects dorsal frontoparietal regions within the DAN. The middle branch (SLF II) links the DAN and VAN by connecting angular gyrus and MFG (Fox et al., 2006; He et al., 2008). The inferior branch (SLF III) connects the supramarginal gyrus with the inferior frontal gyrus, constituting the VAN (Liu et al., 2023; Rojkova et al., 2016). SLF II/III disconnections disrupt DAN-VAN interactions, with right hemisphere (RH) damage leading to left visuospatial neglect (Bartolomeo et al., 2012; Thiebaut De Schotten et al., 2005; 2014; Doricchi et al., 2008; Lunven & Bartolomeo, 2017; Mengotti et al., 2020; Urbanski et al., 2011). Recently, an additional temporo-occipital node has been identified as part of the cortical network supporting endogenous attention (MacLean et al., 2023; Sani et al., 2021). Characterizing oscillatory dynamics that coordinate intra- and inter-regional activity may clarify how neural communication prepares the system for conscious perception, informing the debate on the neural correlates of consciousness (Mashour et al., 2020; Melloni et al., 2023).

We present new analyses of a dataset that examined cueing effects on conscious perception at the source level (Spagna et al., 2022). Here, we focused on pre-target oscillatory dynamics. We studied three oscillatory mechanisms in 16 regions of interest involved in attentional and perceptual processes. The regions included frontoparietal areas linked by branches of the SLF, the temporo-occipital attentional node, and visual cortices. We examined rhythmic attentional scanning (Fries, 2023), theta-gamma phase-amplitude coupling (Fiebelkorn et al., 2018; Helfrich et al., 2018), and communication-through-coherence (Xiong et al., 2023),

because of their established roles in attention and neural communication (Esghaei et al., 2022) and region-specific oscillatory patterns (Ursino & Pirazzini, 2024).

Method

Participants

This study was promoted by the INSERM (C11–49) and approved by the Institutional Review Board of Ile de France I. Among the 19 neurotypical participants that completed the experiment, five had to be excluded due to technical issues during magnetoencephalographic (MEG) recordings (final sample n = 14; age = 24 ± 3.79 years; age range = 20–32 years; 7 M). All participants were right-handed, reported normal or corrected-to-normal vision, and gave written informed consent before participation.

General Overview of the protocol

Participants arrived at the lab, provided written informed consent, and received instructions about the experiment. The study consisted of a calibration session to determine individual contrast thresholds, followed by a practice block and eight task blocks conducted in the MEG recording environment Paris Brain Institute - CENIR neuroimaging platform (https://parisbraininstitute.org/cenir-neuroimaging-platform). The experimental design, task procedure, and data were previously described in Spagna et al. (2022), hence this study follows the same experimental procedure.

Participants sat in a magnetically shielded room while stimuli were presented on a black projection screen positioned ~80 cm away. The experiment was compiled and run using E-Prime software (RRID: SCR_009567; Psychology Software Tools, Pittsburgh, PA) on a Windows XP desktop computer, with a PROPixx projector (resolution: 1050 × 1400 pixels; refresh rate: 60 Hz) displaying the stimuli on a gray background.

Experimental Design

Stimuli and Display

All stimuli were presented on a gray background at the center of a black projection screen using a PROPixx projector (resolution: 1050 × 1400 pixels; refresh rate: 60 Hz) located outside the shielded recording room. The display consisted of three rectangular placeholders, each one occupying 3.6◦ × 4.9◦ of visual angle. One was presented at the center of the screen and contained a black fixation cross. The other two placeholders were positioned at the bottom left and bottom right of the screen, each located 6° laterally and 4° below the central fixation cross. On each trial, a near-threshold Gabor patch target appeared in one of the peripheral placeholders. These stimuli were created with maximum and minimum Michelson contrast of 0.92 (referred to as 100% contrast used in our manipulations) and 0.02 (1%contrast) respectively. We chose to present stimuli in the lower quadrants to optimize MEG responses from early visual areas (Portin et al., 1999) (**Figure 1**).

Task Design

Each trial required participants to complete two sequential behavioral tasks: a tilt discrimination task, in which they judged the orientation of a Gabor patch, and a target detection task, in which they reported whether they had seen a target and, if so, in which visual hemifield it had appeared (**Figure 1a**). Each trial followed this sequence: (1) Fixation display (1000–1500 ms ISI): participants fixated on a central black cross. (2) Cue presentation (50 ms): a black dot (1° diameter, RGB: 128/128/128) appeared near one of the two peripheral placeholders. In 67% of trials (cued condition), the cue appeared near the placeholder where the target would later appear. In the remaining 33% of trials (uncued condition), the cue appeared in the opposite location. Participants were informed that the cue was predictive of the location of the target (ie., in

target-present trials cues likely indicated the target location). (3) Inter-stimulus interval (ISI, 250 ms): a brief delay before target onset. (4) Target presentation (16 ms): a near-threshold Gabor patch (spatial frequency: 5 cycles/degree; diameter: 2.5°; orientation chosen among 12 equally spaced angles between 0° and 180°, excluding vertical and horizontal) appeared in one of the two peripheral placeholders. Second ISI (484 ms): participants maintained fixation before the behavioral response phase began. (5) Tilt discrimination task: participants identified the orientation of the Gabor patch using a response box with three vertical buttons. Two reference orientations were displayed on the screen, 3° apart. Participants pressed the upper button (index finger) for the upper orientation or the middle button (middle finger) for the lower orientation (one of the two always correct, randomized across trials). The third button was not used in this task. After the response to the tilt discrimination task, or after 3 s of no response, (6) Target detection task. Two arrow-like stimuli (>>>>>> or <<<<<<) appeared above and below the fixation cross, with the word "absent" beneath them. Participants responded using the same three-button response box: upper button (index finger): Target seen in the right placeholder. middle button (middle finger): Target seen in the left placeholder. Lower button (ring finger): Target not seen. After a jittered interval between 1–1.5 s delay, the next trial began.

Calibration Block

Prior to the main experiment, participants completed a calibration session (~6 min) to determine the contrast threshold at which the target was detected ~50% of the time. This session ensured that each participant's contrast level was individually adjusted to yield approximately equal proportions of seen and unseen trials. A two-down/one-up psychophysical staircase procedure was used to estimate detection thresholds separately for cued and uncued targets, ensuring a balanced number of trials across the four key experimental conditions (seen-cued,

seen-uncued, unseen-cued, unseen-uncued). Participants performed the same task as described in the Task Design section, except that target contrast varied dynamically based on prior responses.

Experimental Blocks

Following calibration, participants completed eight MEG recording blocks (~8 min per block), for a total of 784 trials, distributed as follows: 448 cued target trials (67%), 224 uncued target trials (33%), and 112 catch trials (no stimulus presented). The procedure is described in the Task Design section.

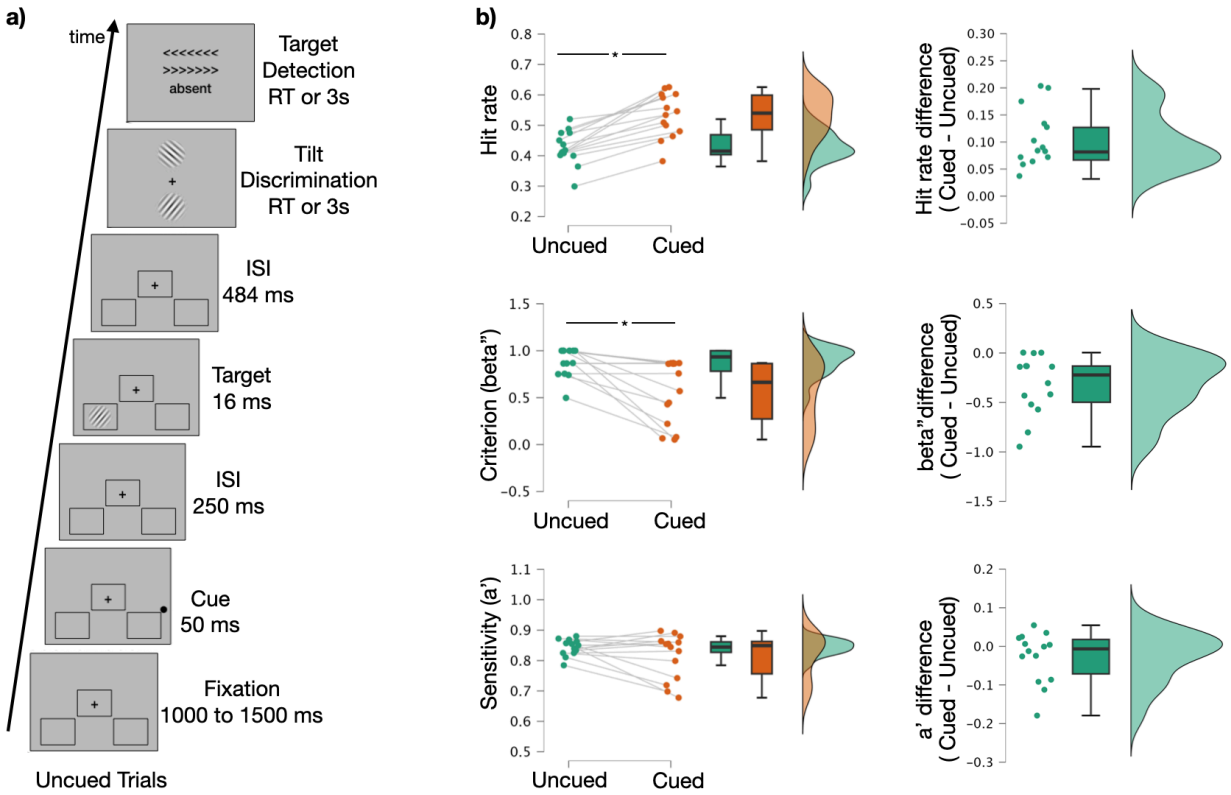

Figure 1. Task design and behavioral results. **a)** Stimulus Sequence: schematic representation of the sequence of events in uncued target trials. The display consisted of three rectangular placeholders: one at the center of the screen containing a black fixation cross and two at the bottom left and bottom right. On each trial, a near-threshold Gabor target appeared in one of the peripheral placeholders, preceded by a supra-threshold visual cue appearing opposite location. In the tilt discrimination task, participants pressed a button to indicate the orientation of the Gabor patch. In the target detection task, participants indicated whether they did not see the target (absent), or whether it had been presented in the left (<<<<<<<) or right (>>>>>>>) target placeholder. **b)** Behavioral Performance: top panel: Hit rates were higher for cued than uncued targets ($p < 0.001$), as shown in the left raincloud plot, with the right plot illustrating the difference. Middle panel: perceptual sensitivity (a') remained comparable across conditions ($p = 0.14$), suggesting that cue validity did not influence sensory evidence accumulation. The left plot shows the distribution of a' values, while the right plot displays the difference between them. Bottom panel: the decision criterion (beta'') was more liberal for cued targets ($p < 0.01$), indicating that cues increased the likelihood of reporting target presence. The left plot depicts the distribution of beta'' values, while the right plot illustrates the difference between conditions. Additional analyses of these datasets (e.g., ANOVAs on accuracy) can be found in our previous study (Spagna et al., 2022).

MRI recordings

High-resolution T1-weighted structural MRI images (MPRAGE sequence, flip-angle, 9; Repetition Time, 2300 ms; Echo Time, 4.18 ms; voxel size: 1 x 1 x 1 mm) were acquired for each participant using a 3-T Siemens, TRIO whole-body MRI scanner (Siemens Medical Solutions, Erlangen, Germany) located at the CENIR MRI center (Paris Brain Institute France). After acquisition, images were segmented using the FreeSurfer "recon-all" pipeline (Fischl, 2012), and imported in Brainstorm (Tadel et al., 2011) for co-registration purposes. MEG sensors and structural MRI images were first manually aligned using the nasion/left ear/right ear (NAS/LPA/RPA) fiducial points recorded in the MEG file and in the MRI MNI coordinates. Co-registration was then further refined using the "refine using head points" option on Brainstorm, an iterative closest point algorithm fitting the head shape and the digitized scalp points. Additional details about the MRI-MEG co-registration steps as done in Brainstorm can be found here (Tadel et al., 2019).

MEG recordings

Continuous MEG recordings were conducted at the CENIR (https://parisbraininstitute.org/cenir-neuroimaging-platform) with an ELEKTA Neuromag TRIUX® machine (204 planar gradiometers and 102 magnetometers) located in a magnetically shielded room with a sampling frequency rate of 1kHz and a bandwidth ranging from of 0.01 to 300 Hz. The recordings were then MaxFiltered (v2.2) (Taulu & Simola, 2006) to attenuate environmental noise, Signal Space Separation (SSS) was then implemented, automatic detection of bad channels was conducted, data were filtered (1 to 250 Hz), and resampled at a rate of 250Hz, and then converted in the Fieldtrip structure (RRID: SCR_004849; http://www.fieldtriptoolbox.org/) (Oostenveld et al., 2011) to conduct further preprocessing and analytic steps. Cardiac activity (electrocardiogram – ECG), and vertical and horizontal Electrooculogram (EOG) signals were also recorded. The exact timing of the presentation of the stimuli onset was adjusted based on the signal from a photodiode positioned in the MEG room, allowing for accurate synchronization of the MEG data with the visual presentation. Signal from the photodiode was used to discard 1) trials with a delay between the trigger and the photodiode greater than 300 ms; 2) trials with a delay between the cue and the target greater than 827 ms; 3) trials in which the delay between the trigger of the cue and the photodiode was greater than 40 ms or smaller than 30 ms, for a total of ~1% of the trials.

Preprocessing and Artifact Rejection.

Additional preprocessing steps were conducted using Fieldtrip, using standard parameters and procedures (Oostenveld et al., 2011). Specifically, we began by conducting an initial visual inspection of the recordings to exclude segments with artifacts and ensure data quality control. EOG recordings from both vertical and horizontal sensors were then used to reject trials in which

eye movements (beyond 3º) occurred. Rejection thresholds for both horizontal and vertical EOG traces were set to ± .66V, corresponding to a deviation greater than 3º of visual angle (and with the target at 6º of visual angle). Trials with excessive eye movements and eye blinks (~10.52% of trials) were rejected offline from the MEG traces. Last, trials contaminated by muscular activity (jump or movement) were rejected manually upon visual inspection (~15%). Out of the 10,796 trials acquired in total, 7,454 trials were analyzed (*right visual field*: seen uncued = 396; seen cued = 1,588; unseen uncued = 812; unseen cued = 920; *left visual field*: seen uncued = 639; seen cued = 1,144; unseen uncued = 576; unseen uncued = 1,379).

Event-Related Magnetic Fields.

We analyzed data from 102 NEUROMAG channels. We used a Matlab (version: 9.13.0 (R2022b), The MathWorks Inc.) script to separate the MEG continuous recordings into 2300 ms-long epochs (ranging from -1000 before the cue and 1300 ms after the cue), and epochs from the eight experimental conditions from each participant were then imported into Brainstorm (Tadel et al., 2011). For each condition, event-related magnetic fields were then averaged (weighted) along their entire length (2300 ms).

Source reconstruction.

Signal amplitudes from the 15,002 cortical elemental dipoles underlying the signals measured by the sensors were then estimated from the epochs using the weighted minimum norm estimation (wMNE) imaging method as implemented in Brainstorm (Tadel et al., 2011). The number of dipoles used in our study is a standard in MEG literature, and is meant to cover the entire cortical surface and its folded anatomy (Tadel et al., 2019). The wMNE method identifies a current source density image fitting the data through the forward model, and then favors solutions that are of minimum energy by using source covariance as a prior. wMNE modeling of

the sources was used because it is considered to be the gold standard in the field, because it balances between a conservative approach in reconstructing sources of MEG signal, with reliable statistical inference across participants, and being computationally efficient (less resource-expensive) (Baillet et al., 2001; Tadel et al., 2019). A noise covariance matrix was estimated for each subject from the recordings using the pre-stimulus interval (-1,000 to -2 ms before the presentation of the cue). Estimating the baseline covariance (i.e, noise covariance) over such an amount of time (approximating one second) allows us to assume a sufficient regularization term of the solution (noise from brain activity at rest thought to be unrelated to our task conditions). The constrained source covariance model was used to model one dipole, oriented normally to the surface, a choice that allows us to study the cortical regions associated with the interaction between attention and consciousness. Further processing conducted on the sources per participant consisted of z-score transformation of the signal with reference to the baseline (from -1,000 to -2 ms). A default value was chosen for the spatial smoothing kernel (FWHM = 3mm), and was then applied on the sources that were then re-interpolated (projected) on a common template (MNI 152).

Regions of Interest (ROIs)

We used a ROI-based approach for three key reasons. First, our primary focus is on the conscious visual perception of attended and unattended targets. Therefore, our analyses included sensory regions and frontoparietal cortices, to thoroughly document the intra-regional and inter-regional communication among neural assemblies known to support visual information processing (Fiebelkorn et al., 2018; Fries, 2023; Helfrich et al., 2018; Liu et al., 2023; Spadone et al., 2021; Spagna et al., 2022; Tosoni et al., 2023; Xiong et al., 2023). Second, frontoparietal networks are frequently implicated in attention and conscious perception (Bartolomeo et al.,

2025; Geng et al., 2019; Helfrich et al., 2018; Liu et al., 2023; Spagna et al., 2022; Szczepanski et al., 2014), making them relevant for investigating the neural mechanisms underlying predictive processing and target detection. Our set of ROIs also included a ventrotemporal attention node and the lateral occipital cortex to corroborate the existence of distinct oscillation patterns during seen and unseen trials in low- and mid-level visual regions, a topic that is still being explored (Esghaei et al., 2022; Melloni et al., 2007). Third, restricting our analyses to predefined ROIs increases statistical power and interpretability, allowing us to test specific hypotheses regarding their functional roles while minimizing the risks associated with whole-brain exploratory analyses and multiple comparison corrections.

ROIs were determined anatomically on the right hemisphere (RH) and the left hemisphere (LH). Each ROI was created using the Scout function on Brainstorm (unconstrained), starting by identifying a seed vertex located in the Brodmann area (BA) and then manually expanding the scout to approximately encompass the whole BA. **Supplementary Table 1** reports the list of seed vertices index, MNI coordinates for each seed vertex, corresponding BA, number of vertices in each ROI and surface area. Six regions were drawn along the boundaries of frontal and parietal projections of the dorsal, intermediate, and ventral branches of the superior longitudinal fasciculus (respectively, SLF I, II, and III). An atlas detailing frontoparietal connections along the SLFs was used to reference which BA to include within each ROI (Rojkova et al., 2016). For the regions pertaining to the SLF I, an ROI in the superior frontal gyrus was defined as the region within BA 8 and BA9 bounded ventrally by the superior frontal sulcus, posteriorly by BA6 and anteriorly by BA10. The parietal projection of the SLF I was defined as the portion of BA 7 bounded between the superior parietal sulcus, posteriorly by BA 19 and anteriorly by BA 40. For the regions pertaining to the SLF II, an ROI

in the middle frontal gyrus was defined as a region within BA 46 and bounded dorsally by the superior frontal sulcus, ventrally by the inferior frontal sulcus of the pars opercularis (BA 44) and pars orbitalis (BA 47), anteriorly by BA10 and posteriorly by the primary motor cortex (BA 4). The parietal projection of the SLF II was defined as the angular gyrus (BA 39). For the regions pertaining to the SLF III, an ROI in the inferior frontal gyrus was defined as encompassing the inferior frontal sulcus from the pars opercularis (BA 44) to the pars orbitalis (BA 47), bounded anteriorly by BA10 and posteriorly by the primary motor cortex (BA 6). The parietal projection of the SLF II was defined as the supramarginal gyrus (BA 40). Two other ROIs were drawn along a previously identified ventro-temporal cortical node (BA 37) associated with attentional control network (MacLean et al., 2023; Sani et al., 2021) and one along the lateral occipital surface encompassing V1 and V2 (BA 17 and BA 18) to monitor effects of attention on the visual cortex. See **Figure 2** and **Supplementary Table 1** for more details about the area included in each ROI.

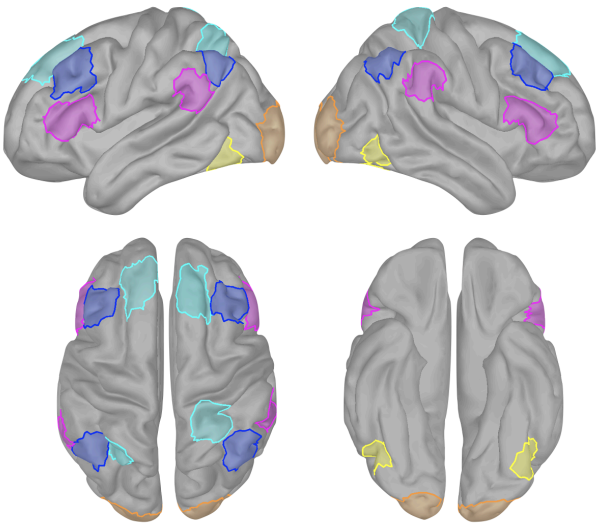

Figure 2. Surface area for each of the 16 regions of interest. The figure displays regions linked by SLF I (teal), SLF II (blue) and SLF III (pink). Orange: early visual cortex (V1 & V2). Yellow: ventro-temporal cortical node.

Supplementary Table 1. Detail regarding how the 16 ROIs were created, including seed vertex and number of vertices included, surface area and Brodmann area number. LH = left hemisphere; RH = right hemisphere.

ROIs	seed vertex index	seed vertex MNI x y z coordinates	region	BA	Number of Vertices included in the ROI	Area (cm2) of the ROI
LH Visual	3625	-18 -101 -2	LO	BA 17 + 18	278	35.82
LH TO Node	3987	-46 -64 -13	LT	BA 37	95	12.86
LH supFron SLF1	2670	-13 47 41	LF	BA 8 + BA 9	165	23.3
LH midFron SLF2	5546	-40 -35 40	LF	BA 46	187	23.63
LH infFron SLF3	1462	-50 37 12	LF	BA 44 + BA 45	161	23.6
LH supPar SLF1	2172	-27 -56 49	LP	BA 7	109	16.48
LH infPar SLF2	2058	-47 -65 50	LP	BA 39	115	19.32
LH TPJ SLF3	5928	-63 -44 26	LP	BA 40	111	16.03
RH Visual	11033	20 -104 -3	RO	BA 17 + 18	285	36.36
RH TO Node	14756	47 59 10	RT	BA 37	93	12.83
RH supFron SLF1	9026	23 26 58	RF	BA 8 + BA 9	165	22.7
RH midFron SLF2	8495	42 29 47	RF	BA 46	170	23.22
RH infFron SLF3	8357	52 37 13	RF	BA 44 + BA 45	160	23.29
RH supPar SLF1	9786	23 -40 63	RP	BA 7	133	22.13
RH infPar SLF2	10614	48 -63 49	RP	BA 39	135	20.33
RH SLF3	10486	68 -32 32	RP	BA 40	100	16.12

Note: We analyzed coherence across a total of 28 pairs of ROIs, including the following combinations: TO_Node x Visual, supFron_SLF1 x Visual, supFron_SLF1 x TO_Node, midFron_SLF2 x Visual, midFron_SLF2 x TO_Node, midFron_SLF2 x supFron_SLF1, infFron_SLF3 x Visual, infFron_SLF3 x TO_Node, infFron_SLF3 x supFron_SLF1, infFron_SLF3 x midFron_SLF2, supPar_SLF1 x Visual, supPar_SLF1 x TO_Node, supPar_SLF1 x supFron_SLF1, supPar_SLF1 x midFron_SLF2, supPar_SLF1 x infFron_SLF3, infPar_SLF2 x Visual, infPar_SLF2 x TO_Node, infPar_SLF2 x supFron_SLF1, infPar_SLF2 x midFron_SLF2, infPar_SLF2 x infFron_SLF3, infPar_SLF2 x supPar_SLF1, TPJ_SLF3 x Visual, TPJ_SLF3 x TO_Node, TPJ_SLF3 x supFron_SLF1, TPJ_SLF3 x midFron_SLF2, TPJ_SLF3 x infFron_SLF3, TPJ_SLF3 x supPar_SLF1, TPJ_SLF3 x infPar_SLF2.

Data Analysis

Behavioral performance

Signal detection theory (SDT) was used to assess perceptual sensitivity (a') and response bias (beta'') based on the spatial relationship between cue and target (cued vs. uncued targets). A' quantifies the signal-to-noise ratio, where values range from 0.5 (chance-level) to 1 (perfect performance), while beta'' reflects response criterion, with values near 1 indicating a conservative approach (fewer false alarms, more misses) and values near -1 indicating a liberal approach (more false alarms).

Target contrast was calibrated to achieve ~50% detection at both valid and invalid locations. Given that some participants made no false alarms, nonparametric SDT measures were used (Pollack & Norman, 1964). We computed the percentage of seen targets (hits) and false alarms (FAs), estimating a' and beta'' separately for cued and uncued trials. Trials were partitioned in seen or unseen based on participants' response to the detection task: seen trials comprised only trials when the participant also reported the correct left/right position of the target (Chica et al., 2010). Differences between conditions were tested using paired-sample t-tests, while Wilcoxon signed-rank tests assessed potential differences in threshold sampling during calibration. Additional analyses of these datasets (e.g., ANOVAs on accuracy) can be found in our previous study (Spagna et al., 2022).

$$A' = 0.5 + \frac{(\text{Hits} - \text{FAs}) * (1 + \text{Hits} - \text{FAs})}{4 * \text{Hits} * (1 - \text{FAs})};$$

$$Beta'' = \frac{\text{Hits} * (1 - \text{Hits}) - \text{FAs} * (1 - \text{FAs})}{\text{Hits} * (1 - \text{Hits}) + \text{FAs} * (1 - \text{FAs})}.$$

Gamma activity within each ROI

Time-frequency decomposition using Morlet wavelets was conducted on source level signals to compute the mean magnitude of gamma (30 - 90Hz) activity separately for each ROI. The mask for each ROI was applied before extracting the signal, reducing computation time. The time window for this analysis was restricted to the cue-target interval (from 0 to 300 ms) because of our interest in examining the dynamics observed immediately after a visual cue and their role in conscious processing of an impending target. Gamma frequency band was binned into 7 bins of 10 Hz each,

We conducted an ANOVA with the factors of Report (seen, unseen) x Cueing (cued, uncued) x Time (150 consecutive 2-ms intervals from 0 to 300ms) x Frequency (7 10-Hz bin: 30 - 90Hz) separately on each ROI (16: Left Visual, Left TO Node, Left supFron_SLF1, Left midFron_SLF2, Left infFron_SLF3, Left supPar_SLF1, Left infPar_SLF2, Left TPJ_SLF3, Right Visual, Right TO Node, Right supFron_SLF1, Right midFron_SLF2, Right infFron_SLF3, Right supPar_SLF1, Right infPar_SLF2, Right TPJ_SLF3) using JASP (version 0.18.3). Significant four-way interactions were further analyzed using follow-up contrasts for each ROI: (1) [Seen *vs* Unseen], allowing us to identify whether gamma oscillations changed based on conscious report; (2) [Seen Cued *vs* Unseen Cued] and [Seen Uncued *vs* Unseen Uncued] to identify changes in gamma oscillations based on conscious report and cueing effect. For each contrast, we corrected for multiple comparisons among timepoints using paired *t*-tests with 5000 permutations, a two-tailed significance threshold of .05, and Bonferroni-correction (adjusted $p = 0.0006$, with 151 time points). Additionally, we used the function on Brainstorm to control for false discovery rate at alpha=0.05.

Phase-Amplitude Coupling within each ROI

To examine whether participants' attentional behavior modulates cross-frequency coupling, we estimated the strength of the coupling between theta phase and gamma amplitude (phase-amplitude coupling, PAC) (Canolty & Knight, 2010; Voytek, 2010) separately for each participant, task condition (seen cued, seen uncued, unseen cued, and unseen uncued) and ROI. We began by estimating PAC on the source signals (details reported in the source reconstruction section) of each ROI using the scout function implemented in Brainstorm applied before the PAC process, so that only the resulting scout time series were evaluated for PAC coupling, reducing compute time. We filtered the raw signals from each ROI twice: once within the theta frequency range (4 - 8Hz) and once at the gamma frequency range (30 - 90 Hz). We then estimated the instantaneous phase for the theta frequency time series using the complex option on Brainstorm, and then the amplitude of the gamma frequency time series. Because we were interested in the attentional dynamics during the cue-target interval, we extracted PAC signals during the period between the cue presentation until 300 ms after using custom code on MATLAB (version 2022b, The Mathworks, Natick, MA). We submitted PAC values from the comodulograms for the four task conditions to a four-way ANOVA with the factors Report (seen, unseen) x Cueing (cued, uncued) x 5 (Theta: 4Hz, 4.96Hz, 5.94Hz, 6.93Hz, 7.94Hz) × 22 (Gamma: 31–89 Hz) on JASP (version 0.18.3). We further examined significant four-way interactions with follow-up ANOVAs using a Report x Cueing x Theta x Gamma design, dividing the gamma range into 10Hz bins (seven separate analyses from 30 to 90Hz). For gamma bins showing a significant Report x Cueing x Theta interaction, we conducted planned post-hoc comparisons (two-tailed, alpha = .05), applying Holm–Bonferroni correction to adjust for multiple comparisons.

Coherence among ROIs

The linear relationship of signals from pairs of ROIs in the gamma band (30-90 Hz) was indexed by the covariance of two signals in the frequency domain using complex coherence (Brookes et al., 2011; Xiong et al., 2023). The mask for each ROI was applied before extracting the mean signal. The magnitude of gamma-band coherence was estimated from Morlet wavelets and analyzed separately for the 7 bins of (30-90; 10 Hz each). The time window for this analysis was restricted to the cue-target interval (from 0 to 300 ms), divided into 5 100 ms-long windows with a percentage of overlap set to 50% (49 ms, 99 ms, 149 ms, 199 ms, 249 ms). As cross-hemispheric communication between ROIs was not the focus of this manuscript, we analysed RH and LH ROIs separately to reduce computation time and limit the false discovery rate associated with multiple comparisons. To examine significant differences between contrasts of interest (e.g., gamma coherence in a pair of ROIs for *seen* compared *unseen* trials), we conducted a Report (seen, unseen) x Cueing (cued, uncued) x ROIPair (28 pairs, see Supplementary Table 1) x Frequency (30-90Hz, in 10Hz bins) ANOVA separately for each time window (49ms, 99ms, 149ms, 199ms, 249ms) on JASP (version 0.18.3). We conducted analysis of coherence separately for ROIs within the left and right hemisphere. We further explored significant interactions using planned follow-up contrasts for each ROI pair: (1) [Seen *vs* Unseen], to assess changes in gamma coherence based on conscious report; (2) [Seen Cued *vs* Unseen Cued] and (3) [Seen Uncued *vs* Unseen Uncued] to identify the combined effect of conscious report and cuing. We corrected for multiple comparisons across frequency bins Bonferroni correction (adjusted p = 0.007, based on 7 frequency bins), and controlled for the false discovery rate at alpha=0.05 (two-tailed)).

Results

Decision criterion shifts for cued targets

Hit rates were higher for cued (M = 0.53, SD = 0.07) than uncued (M = 0.43, SD = 0.06), ($t(13) = 7.57$, $p < 0.01$) targets. Perceptual sensitivity (a') remained comparable for cued (M = 0.82, SD = 0.08) and uncued targets (M = 0.84, SD = 0.03), ($t(13) = 1.57$, $p = 0.14$), suggesting that cue validity did not affect sensory evidence accumulation. However, participants adopted a more liberal criterion for cued targets (M = 0.56, SD = 0.34) compared to uncued targets (M = 0.88, SD = 0.15), ($t(13) = 3.99$, $p < 0.01$), suggesting that cues biased decision-making, making participants more likely to report target presence after valid cues (**Figure 1**).

Gamma oscillations in RH superior frontal gyrus associated with conscious reports

We began by examining the role of gamma oscillations in conscious report.

The four-way interaction (Report x Cueing x Time x Frequency) reached statistical significance for the following regions: Right supFron SLF 1: ($F(900, 11700) = 1.26$; $p < .001$; $\eta_p^2 = .09$), Right midFron SLF 2: ($F(900, 11700) = 1.23$; $p < .001$; $\eta_p^2 = .09$), Right supPar SLF1: ($F(900, 11700) = 1.55$; $p < .001$; $\eta_p^2 = .09$), Right infPar SLF2: ($F(900, 11700) = 1.17$; $p < .001$; $\eta_p^2 = .08$), RightTPJSFL3: ($F(900, 11700) = 1.20$; $p <.001$; $\eta_p^2 = .09$), Left Visual: ($F(900, 11700) = 1.12$; $p < .05$; $\eta_p^2 = .08$), Left Node: ($F(900, 11700) = 1.62$; $p <.001$; $\eta_p^2 = .11$), LeftTPJSFL3: ($F(900, 11700) = 1.30$; $p <.001$; $\eta_p^2 = .09$), Left supPar SLF1: ($F(900, 11700) = 1.45$; $p < .001$; $\eta_p^2 = .10$). The interaction did not reach statistical significance for the Right Visual: ($F(900, 11700) = 1.07$; $p = .07$; $\eta_p^2 = .08$), Right TONode: ($F(900, 11700) = 0.91$; $p = .97$; $\eta_p^2 = .07$), Right infFron SLF3: ($F(900, 11700) = 1.00$; $p = .48$; $\eta_p^2 = .07$), Left supFron SLF 1: ($F(900, 11700) = 1.23$; $p = .31$; $\eta_p^2 = .06$), Left midFron SLF 2: ($F(900, 11700) = 0.62$; $p = .99$; $\eta_p^2 = .04$), Left infFron SLF 3: ($F(900, 11700) = 0.71$; $p = .99$; $\eta_p^2 = .05$), and Left infPar SLF2:

($F(900, 11700) = 1.23$; $p = .31$; $\eta_p^2 = .07$)

We further analyzed significant four-way interactions for each ROI using the follow-up contrast Seen vs. Unseen to assess gamma oscillation changes based on conscious reports. Results showed that the RH superior frontal gyrus was the only region showing greater gamma activity before seen targets than unseen targets ($t(13) = 3.36$, $p_{FDR} = .001$, Cohen's $d = .90$). This difference emerged in the 60 Hz frequency bin between 170 and 200 ms post-cue (**Figure 3a**) and remained significant even after excluding one participant with particularly large amplitudes in both conditions ($t(12) = 4.72$, $p_{FDR} = .001$, Cohen's $d = 1.31$). Follow-up analyses confirmed that this increased gamma activity (170–200 ms) was independent of cue or target side (all ps < .05). These findings suggest that gamma oscillations in the prefrontal node of the RH SLF I during the cue-target interval may have engaged attentional mechanisms supporting conscious processing of an impending target, regardless of cue or target location.

Additional follow-up analyses identified another time window (~100 ms, 20 ms duration) in which gamma oscillations in the 60 Hz bin in the RH superior frontal gyrus were larger before seen targets than unseen targets ($t(13) = 2.36$, $p < .05$, Cohen's $d = .63$), but only for contralateral cues and targets (i.e., in the left visual field; see **Figure 3**, first red area). This finding aligns with prior evidence suggesting the early involvement of this region specifically in directing attention to the left visual field (Shulman et al., 2010).

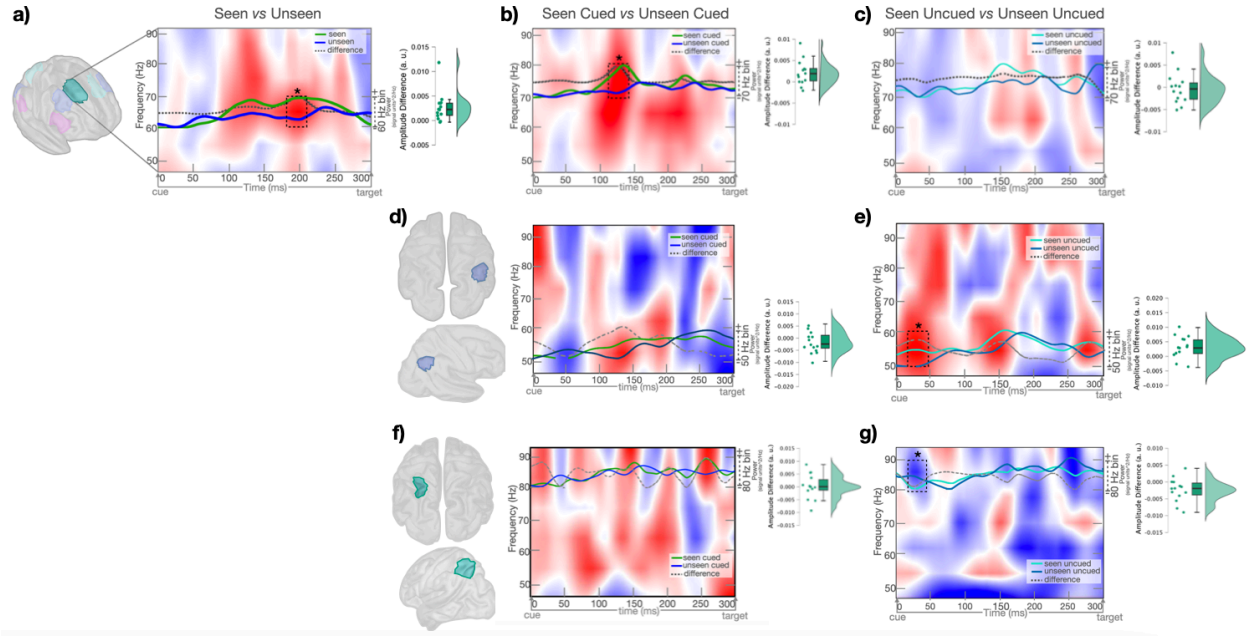

Figure 3. (a) Left: Region of interest in the right hemisphere (RH) superior frontal gyrus. Middle: Time-frequency decomposition of gamma activity (50–90 Hz) from cue onset (0 ms) to target presentation (300 ms). Gamma oscillations at 60 Hz were greater for seen (solid red) vs. unseen (solid blue) targets, with a significant difference (dotted gray line) observed in the 170–200 ms window. Right: Individual subject amplitude differences in the 60 Hz bin for Seen vs. Unseen trials (170–200 ms). **(b)** Time-frequency decomposition showing greater 70 Hz gamma activity for seen-cued (solid red) vs. unseen-cued (solid blue) targets, with a significant difference (dotted gray line) in the 120–140 ms window. Right: Individual subject amplitude differences in the 70 Hz bin for Seen Cued vs. Unseen Cued trials (120–140 ms). **(c)** Region of interest in the RH intraparietal sulcus. Time-frequency decomposition for Seen Uncued vs. Unseen Uncued trials, showing no significant differences. **(d)** Time-frequency decomposition showing no significant difference in the 50 Hz bin for seen-cued (solid red) vs. unseen-cued (solid blue) targets. Right: Individual subject amplitude differences in the 50 Hz bin for Seen Cued vs. Unseen Cued trials. **(e)** Time-frequency decomposition for Seen Uncued vs. Unseen Uncued trials, revealing a significant difference (dotted gray line) in the 20–50 ms window at 50 Hz. Right: Individual subject amplitude differences in the 50 Hz bin for Seen Uncued vs. Unseen Uncued trials. **(f)** Region of interest in the left hemisphere (LH) superior parietal lobule. Time-frequency decomposition showing no significant difference in the 80 Hz bin for seen-cued (solid red) vs. unseen-cued (solid blue) targets. Right: Individual subject amplitude differences in the 80 Hz bin for Seen Cued vs. Unseen Cued trials. **(g)** Time-frequency decomposition for Seen Uncued vs. Unseen Uncued trials, showing a significant difference for Unseen Uncued compared to Seen Uncued trials (dotted gray line) in the 20–50 ms window at 80 Hz. Right: Individual subject amplitude differences in the 80 Hz bin for Unseen Uncued vs. Seen Uncued trials. Asterisks (*) above dotted rectangular boxes indicate statistically significant differences.

We further analyzed significant four-way interactions for each ROI using the follow-up contrasts Seen Cued vs. Unseen Cued and Seen Uncued vs. Unseen Uncued to evaluate the effects of cueing on conscious reports. Gamma activity in the RH superior frontal gyrus differed between conscious reports of cued targets ($t(13) = 2.68$, $p < .05$, Cohen's $d = .72$; **Figure 3b**) but not of uncued targets ($t(13) = -0.33$, $p = .74$, Cohen's $d = -.09$; **Figure 3c**). This effect occurred in the 70 Hz bin between 120 and 140 ms post-cue. Follow-up analyses revealed that cued targets presented on the left visual field were associated with greater gamma oscillation in the RH superior frontal gyrus for seen vs. unseen targets earlier in time (40–140 ms) compared to cued targets presented on the right visual field (120–150 ms). Because the difference between seen and unseen trails was statistically significant only for cued but not uncued targets, this reflects a *spatial* attention mechanism (Carrasco & Barbot, 2019; Denison et al., 2019; Fernández et al., 2019). No other region showed a significant difference between Seen Cued and Unseen Cued trials. Altogether, these findings suggest that gamma oscillations in the RH frontal node during the cue-target interval activated spatial orienting mechanisms across the entire visual field.

For uncued targets, the contrast between seen and unseen trials was associated with increased gamma activity at 50 Hz in the RH intraparietal sulcus for uncued targets ($t(13) = 3.23$, $p < .05$, Cohen's $d = .86$; **Figure 3d**). This contrast did not reach significance for cued targets ($t(13) = -1.08$, $p = .30$, Cohen's $d = -.29$; **Figure 3e**). Conversely, gamma activity at 80Hz in the LH superior parietal region was greater for unseen uncued targets compared to seen uncued targets ($t(13) = -3.26$, $p < .05$, Cohen's $d = -.87$; **Figure 3f**), while this difference was not statistically significant for cued targets ($t(13) = 0.13$, $p = .89$, Cohen's $d = -.04$; **Figure 3g**). No other region showed a significant difference between Seen Uncued and Unseen Uncued trials. Altogether, these findings suggest a hemispheric asymmetry in how nodes in the parietal cortex

support conscious perception of uncued targets early in the cue-target period. Specifically, when targets are uncued, gamma activity in the right intraparietal sulcus appears to facilitate conscious report, whereas similar activity in the left superior parietal lobule seems to hinder it.

Theta-gamma phase-amplitude coupling in a right-lateralized superior parietal ROI is associated with conscious reports.

To examine the relationship between theta-gamma coupling and conscious processing of impending near-threshold visual targets, we conducted a 2 (Report: Seen, Unseen) × 2 (Cueing: cued targets, uncued targets) × 5 (Theta: 4–8 Hz) × 22 (Gamma: 31–89 Hz) ANOVA on PAC values from each ROI. We begin by focusing on the RH superior parietal lobe due to its established role in attentional orienting (Sczepanski et al., 2014; Helfrich et al., 2018; Fiebelkorn et al., 2018; Fiebelkorn & Kastner, 2019). As expected, we observed a four-way interaction in the RH superior parietal ROI ($F(84, 1092) = 2.01$; $p < .01$; $\eta_p^2 = .13$), indicating that theta-gamma PAC in the RH superior parietal lobe changes as a function of cueing or frequency-specific modulations. To further characterize this interaction, we conducted follow-up 2 (Report: Seen, Unseen) x 2 (Cueing: cued targets, uncued targets) ANOVAs separately for each of Theta frequency bins and across six 10Hz Gamma frequency bins. A significant Report x Cueing interaction emerged in the 6 Hz Theta and 40 Hz bins Gamma ($F_{(1, 13)} = 8.59$; $p < .01$; $\eta_p^2 = .40$) **(Figure 4)**. Post-hoc comparisons revealed that PAC values for cued targets were significantly greater comparing Seen (mean .20 ± .01) and Unseen trials (mean .14 ± .01; $t(13) = 3.44$; $p_{holm} < .01$ adjusted for comparing a family of 6), but not for uncued targets (Seen: mean .16 ± .01; Unseen mean .19 ± .01; $t(13) = -1.39$; $p_{holm} = .53$). No other pairwise comparisons reached significance ($p_{holm} > .12$). The main effect of the factor Conscious Report failed to reach significance ($F(1,13) = 1.43$, $p = .25$; $\eta_p^2 = .10$), suggesting that PAC in the RH superior parietal

lobe does not uniformly tag conscious perception. We did not observe significant Report x Cueing interactions on PAC values from any other level of theta and gamma frequency bin. Last, the four-way interaction was not significant for any of the other ROIs in the ipsilateral frontal lobe (RH MFG: $F(84, 1092) = 0.91$; $p = .69$; $\eta_p^2 = .07$; RH SFG: $F(84, 1092) = 1.64$; $p = .06$; $\eta_p^2 = .11$;) or in the LH homologous region (LH SupPar = $F(84, 1092) = 0.89$; $p = .73$; $\eta_p^2 = .06$).

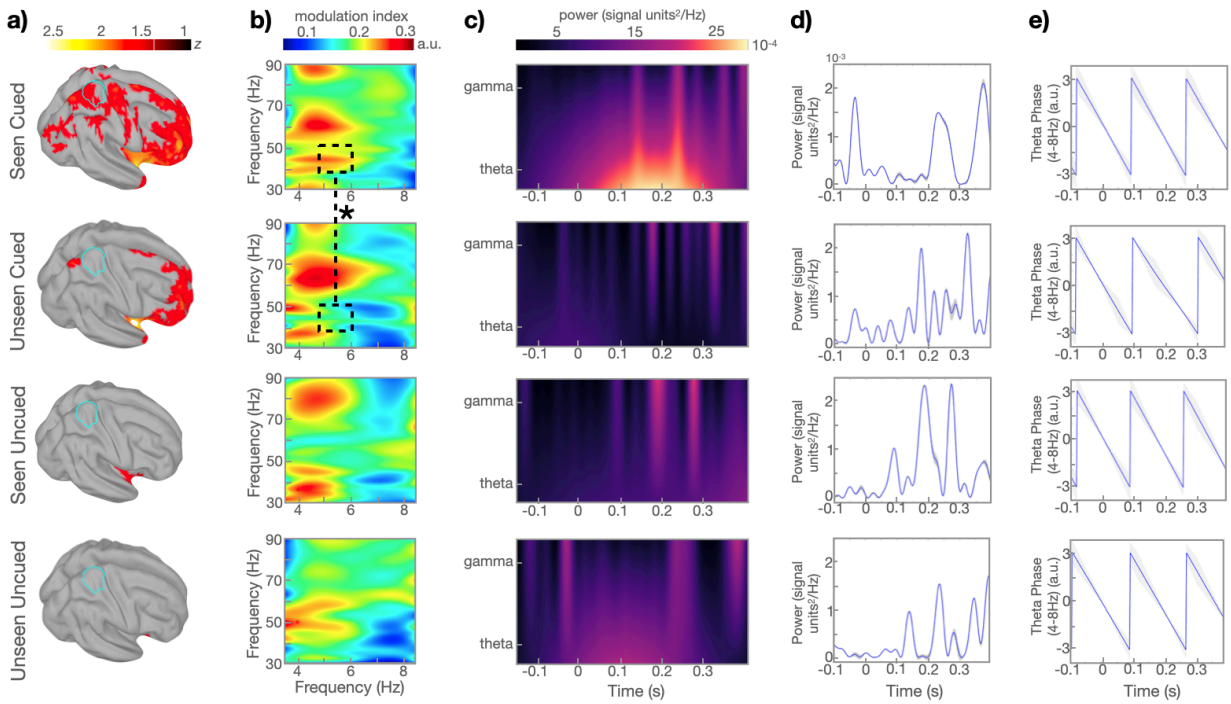

Figure 4. We estimated the following measures during the cue-target interval, separately for each task condition (top row: seen-cued; second row: unseen-cued; third row: seen-uncued; bottom row: unseen-uncued): **a)** location of the RH superior parietal ROI (outline in teal) and whole-brain activity for each of the four task conditions. **b)** Phase amplitude coupling (PAC) between theta (4-8Hz) and gamma (30-90Hz) frequency bands. **c)** Time-frequency decomposition analysis using the Hilbert transform on the gamma and theta frequency bands during the cue-target interval. **d)** Time series of the gamma power spectrum. The shaded area represents the standard error of the mean. **e)** Time series of the theta phase during the cue-target interval. The shaded area (in light gray) represents the standard error of the mean. We conducted statistical analyses only on the PAC values shown in the comodulograms (b), while the other panels (a, c–e) are provided for visualization. Theta-gamma coupling in the RH superior parietal ROI was significantly greater for seen vs. unseen cued targets ($p < .01$), but not for uncued targets. Asterisks (*) indicate statistically significant differences.

Gamma coherence associated with conscious reports in frontoparietal regions

We begin by discussing the temporal evolution of gamma coherence in conscious report among pairs of ROIs in the RH. The three-way interaction (Report x Cueing x ROIPairs) was significant in all five time windows (49 ms: $F(27, 351) = 10.42$, $p < .001$, $\eta_p^2 = .88$; 99 ms: $F(27, 351) = 10.73$, $p < .001$, $\eta_p^2 = .45$; 149 ms: $F(27, 351) = 13.14$, $p < .001$, $\eta_p^2 = .50$; 199 ms: $F(27,$

351) = 10.13, $p < .001$, $\eta_p^2 = .44$; 249 ms: $F(27, 351) = 9.80$, $p < .001$, $\eta_p^2 = .43$). Gamma-rhythmic synchronization, estimated through signal coherence during the cue-target interval, was significantly greater for seen compared to unseen targets between the RH superior and middle frontal gyri in the 149 ms time-window and 30 Hz frequency bin (**Figure 5a**) ($t(13) = 3.30$, $p < .01$, Cohen's $d = .88$). No other coherence contrasts among regions in the RH reached statistical significance during this period. This effect remained significant even after excluding one participant with an exceptionally high coherence difference across conditions ($t(13) = 2.55$, $p < .05$, Cohen's $d = .68$). Note that this was not the same participant with an extreme value in the oscillation analyses. Paralleling the approach used to analyze the gamma oscillations, we conducted follow-up analyses to examine whether the increase in coherence associated with conscious reports differed between cued and uncued targets. We observed no significant difference for cued targets across all time windows (**Figure 5b**). However, coherence between the RH superior and middle frontal gyri was significantly greater for seen vs. unseen trials when the target was uncued. This effect was found observed during two consecutive time windows (149 ms: $t(13) = 2.72$; $p < .01$; Cohen's $d = .73$; 199 ms: $t(13) = 3.00$; $p < .01$; Cohen's $d = .80$) (**Figure 5c**). Additionally, we observed greater coherence between the superior frontal gyrus and the superior parietal gyrus was also significantly greater for seen vs. unseen trials when the target was uncued during the 109 ms time window ($t(13) = 2.94$; $p < .01$; Cohen's $d = .79$) (not shown in the figure). These findings suggest that visuospatial predictive cues enhance conscious processing of an impending target through RH frontoparietal crosstalk, specifically in response to the rare occurrence of uncued targets.

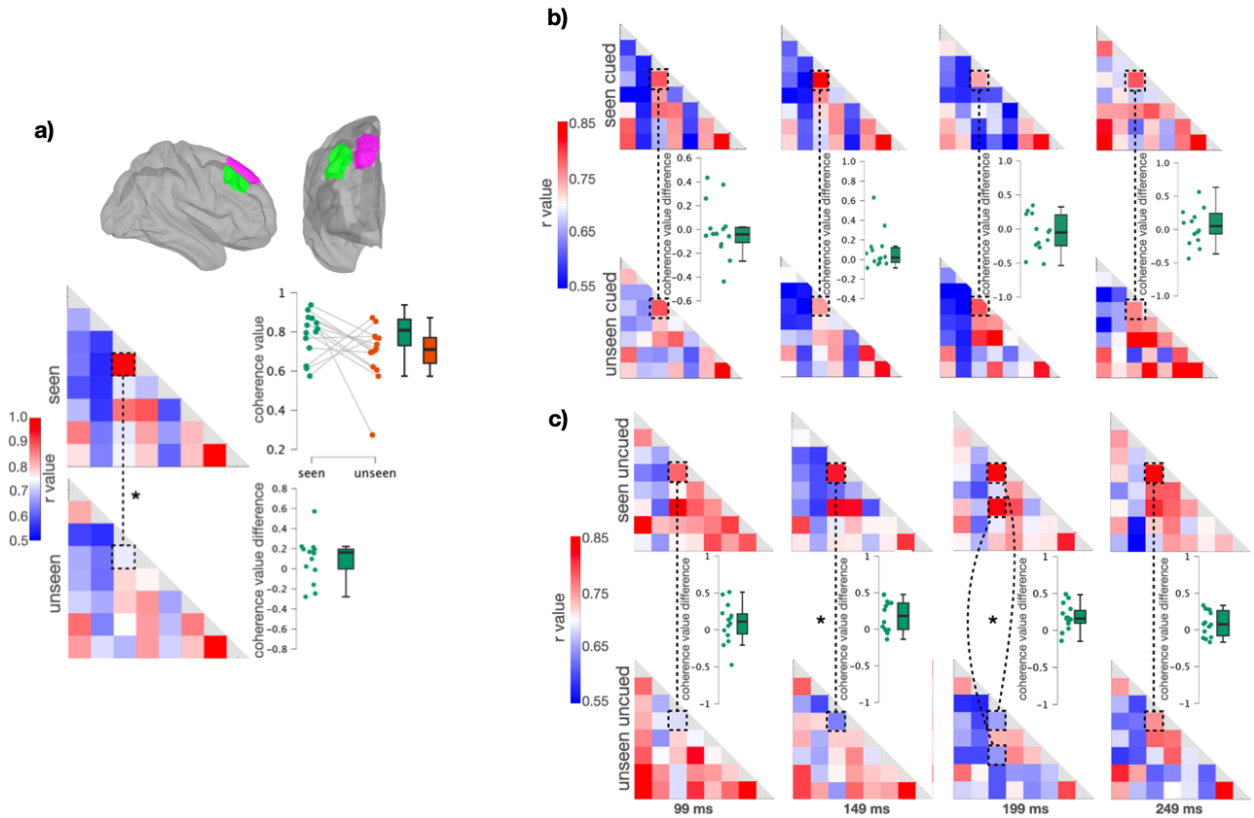

Figure 5. (a) Left: Gamma coherence (30 Hz bin) between the RH superior (pink) and middle (green) frontal gyri, estimated around 150 ms post-cue (50 ms overlap). The top matrix represents coherence values for seen targets, while the bottom matrix represents unseen targets. Top-right panel: Correlation values for each participant in seen and unseen trials. Bottom-right panel: Difference in coherence values between seen and unseen trials. (b) Coherence values across four consecutive time windows post-cue (99 ms, 149 ms, 199 ms, 249 ms). Top row: Seen-cued condition. Bottom row: Unseen-cued condition. (c) Coherence values across four consecutive time windows post-cue (99 ms, 149 ms, 199 ms, 249 ms). Top row: Seen-uncued condition. Bottom row: Unseen-uncued condition. Asterisks (*) indicate statistically significant differences.

Gamma coherence in conscious report among pairs of ROIs in the LH followed a difference pattern. The three-way interaction (Report x Cueing x ROIPairs) was significant only in the last two time windows (49ms: $F(27, 351) = 0.87$, $p = .66$, $\eta_p^2 = .06$; 99ms: $F(27, 351) = 1.06$, $p = .40$, $\eta_p^2 = .08$; 149ms: $F(27, 351) = 1.27$, $p = .17$, $\eta_p^2 = .09$; 199ms: $F(27, 351) = 2.03$, $p < .005$, $\eta_p^2 = .14$; 249ms: $F(27, 351) = 1.57$, $p < .05$, $\eta_p^2 = .11$). Follow up analyses showed that coherence during the cue-target interval was greater for unseen vs. seen targets among

left-lateralized regions. We observed greater coherence between (1) the left middle frontal gyrus and left temporo-occipital (TO) node (199 ms time window; 60 Hz; $t(13) = -3.56$; $p < .01$; Cohen's $d = .95$); (2) the left TO node and left visual cortex (199 ms time window; 70 Hz; $t(13) = -3.56$; $p < .01$; Cohen's $d = .95$); (3) the LH TPJ and superior frontal gyrus (199 ms time window; 70 Hz; $t(13) = -3.71$; $p < .01$; Cohen's $d = .99$); (4) the left TO node and left visual cortex (249 ms time window; 30 Hz; $t(13) = -3.27$; $p < .01$; Cohen's $d = .87$). Altogether, these results indicated that gamma coherence among fronto-temporal, fronto-parietal, and temporo-occipital regions in the LH during the cue-target interval can disrupt conscious report. Two results warrant further investigation: first, the left TO node was involved in three out of the four observed contrasts, highlighting its potential role in attentional reorienting. Second, we observed sustained coherence between left visual and TO nodes across both the 199 ms and 249 ms time windows, with greater coherence for unseen vs. seen trials.

To examine whether these coherence patterns (ie., greater coherence for unseen vs. seen trials) were varied based on the cue manipulation, we conducted follow-up analyses separately for cued targets and uncued targets. (1) Left middle frontal gyrus – left TO node (199 ms, 60 Hz bin): Coherence was greater for unseen targets vs. seen trials when the target was cued ($t(13) = -3.02$, $p < .01$; Cohen's $d = .81$), but not for uncued targets. (2) Left TO node – left visual cortex (199 ms, 70 Hz bin): Coherence was greater for unseen vs. seen trials for cued targets ($t(13) = -3.56$, $i < .01$; Cohen's $d = .95$), but not for uncued targets. (3) LH TPJ – superior frontal gyrus (199 ms, 70 Hz bin): Coherence was greater for unseen vs. seen trials when the target was uncued ($t(13) = -3.08$, $p < .01$; Cohen's $d = .82$), but not when the target was cued. (4) Left TO node – left visual cortex (249 ms, 90 Hz bin): Coherence was greater for unseen vs. seen trials when the target was uncued ($t(13) = -3.41$, $p < .01$; Cohen's $d = .91$) but not when it was cued.

These findings suggest that increased gamma-range coherence among left-lateralized regions disrupts conscious processing of cued and uncued visual targets.

Discussion

We describe how three distinct oscillatory mechanisms in hemisphere-asymmetric frontoparietal regions precede conscious reports of impending near-threshold targets. Neuronal oscillations are an emergent property of the interplay between excitatory and inhibitory neurons within a brain region (Fries, 2023), with different networks exhibiting distinct neural rhythms (Esghaei et al., 2022). Synchronization between these rhythms facilitates efficient information transfer (Fries, 2015). By examining gamma oscillations, theta-gamma phase-amplitude coupling (PAC), and gamma coherence in frontoparietal regions, we uncover hemisphere-asymmetric spectrotemporal dynamics underlying attentional shifts across visual fields. Using magnetoencephalography and a Posner-like visuospatial cueing paradigm, we identified gamma oscillations in the RH SFG predicting conscious reports of cued targets but not uncued targets, supporting their role in anticipatory mechanisms for conscious perception, extending previous finding on attention (Fries, 2023; Szczepanski et al., 2014). Further, PAC in the RH superior parietal lobe predicted conscious reports of cued targets even before target onset (Fiebelkorn et al., 2018; Helfrich et al., 2018). Moreover, our results reveal a circuit-specific mechanism centered on right parietal regions that supports attentional allocation in space (Behrmann et al., 2004; Buschman & Miller, 2007; Vandenberghe et al., 2012). Also, gamma oscillations in the RH intraparietal sulcus and gamma coherence between RH superior and middle frontal gyri preceded conscious report of uncued targets, revealing a parietal “lookout” mechanism anticipating unexpected stimuli (Liu, et al., 2023). This supports the proposal that coupling between DAN-VAN supports attentional reorienting (Fries, 2023; Proskovec et al., 2018; Xiong

et al., 2023). Finally, higher gamma oscillations in the LH superior parietal lobule and coherence in the left-hemisphere frontoparietal networks preceded unreported targets, suggesting a pre-target bias contributing to omission errors (Bartolomeo et al., 2025). This aligns with MEG findings in left neglect patients, where left frontal activity preceded failure to respond to left-sided targets (Rastelli et al., 2013).

Altogether, these results expand recent meta-analytical and intracranial electrophysiology findings that highlight the central role of right-lateralized frontoparietal networks preceding conscious reports (Bartolomeo et al., 2025; Liu, et al., 2023; MacLean et al., 2023; Seidel Malkinson et al., 2024).

Right-lateralized gamma oscillations facilitate attentional scanning

There is broad agreement on the essential role of oscillatory activity in shaping perception and adaptive behavior (Fries, 2023; Nobre & Van Ede, 2023), yet the precise spectral signatures underlying visuospatial attention remain debated (Spadone et al., 2021). Our findings reveal that gamma-band oscillations in the right superior frontal gyrus during the cue-target interval precede conscious reports, with no corresponding effect in the contralateral homologous region. This right-lateralized activity suggests that spatial orienting mechanisms in the superior frontal gyrus operate across the entire visual field, allowing attention to be allocated based on predictive cues. These results reinforce the hypothesis of a specific role of right-hemisphere SLF circuits in attentional orienting, and align with models positing that the right hemisphere integrates spatially relevant information across both hemifields (Bartolomeo et al., 2025), particularly when preparatory mechanisms are engaged (Nobre, 2001). As a key node of the DAN (Corbetta et al., 2008; Tosoni et al., 2023), the right superior frontal gyrus is involved in attentional shifts and rhythmic scanning (Fries, 2023). Our findings strongly suggest that gamma

oscillations in this region serve as a neural mechanism for spatial orienting, regardless of hemifield. Notably, these oscillations were selectively enhanced for impending seen vs. unseen targets, indicating a role in preparing the attentional system for conscious target processing.

Our finding suggests that the DAN may not be as strictly bilaterally organized as often assumed (Corbetta et al., 2008; Shulman et al., 2010), and that hemispheric asymmetries in attentional control extend beyond the VAN (Nobre, 2001). Independent converging evidence for such asymmetries favoring the RH comes from resting-state connectivity studies, which reveal a bias for the left hemisphere to interact primarily with itself, while the RH integrates information both locally and across hemispheres (Gotts et al., 2013). Anatomically, this asymmetry is reinforced by evidence that right-lateralized attention networks are more influenced by external stimuli via primary sensory cortices compared to their left counterparts (Ben Messaoud et al., 2025).

The RH intraparietal sulcus has long been implicated in spatial attention control and attentional reorienting (Corbetta et al., 2008; Szczepanski et al., 2010). The observed increase in gamma activity for seen uncued targets suggests that this region supports preparation for attentional reallocation in case the initial focus of attention is misdirected. This finding confirms human intracerebral results suggesting the existence of a RH “lookout” mechanism (Liu et al., 2023) involved in monitoring for unexpected relevant stimuli and in rapidly redirecting attention to them. In contrast, increased gamma activity at 80 Hz in the LH superior parietal lobule for unseen uncued targets suggests that this region may interfere with or delay the reallocation of attention, reducing the likelihood of conscious perception. This pattern aligns with findings from studies on hemispatial neglect (Rastelli et al., 2013; Bartolomeo et al., 2025), and indicate that

this activity may reflect a maladaptive persistence of attentional bias toward the originally cued location, limiting reorienting to the uncued target.

Theta-Gamma phase-amplitude coupling in the right superior parietal lobe predicts conscious reports

Our results suggest that theta rhythms in parietal regions orchestrate gamma bursts to enhance the representation of attended stimuli, helping maintain attentional selection at behaviorally relevant locations (Fiebelkorn & Kastner, 2019). This provides support for the rhythmic attentional scanning model (Fries, 2023), in which theta-gamma cross-frequency coupling optimizes the allocation of limited neural resources to enhance perceptual selection (Fries, 2023). This is crucial because information processing is limited by the energetic cost of cortical computations (Carrasco and Barbot, 2019). We show that enhanced theta-gamma PAC in the RH superior parietal lobe increases conscious report of cued but not uncued targets, reinforcing the role of parietal cross-frequency coupling in preparatory attention. This aligns with findings that theta rhythms in the frontoparietal network modulate perceptual performance through excitability fluctuations (Helfrich et al., 2018), suppress distractors (Asanowicz et al., 2023), and support attentional shifts (Senoussi et al., 2019).

Importantly, our results extend prior knowledge by demonstrating that PAC operates not only in the post-target period (Canolty & Knight, 2010; Helfrich et al., 2018) but also before target presentation. We show that this process occurs in the RH parietal region, an attention node (Shomstein, 2012; Shomstein & Gottlieb, 2016), where it may enhance attentional sampling and stabilize visual representations across the visual fields, increasing the likelihood of stimulus detection.

Inter-regional communication through gamma coherence prepares for attentional reorienting

Our previous work (Spagna et al., 2022) revealed that frontoparietal engagement was delayed by 40-ms uncued versus cued targets, suggesting an attentional cost of reorienting. This cost may reflect the communication between the DAN and VAN needed to redirect attention (Corbetta et al., 2008). Supporting this interpretation, here we found that gamma coherence between the RH superior and middle frontal gyri predicted conscious reports of uncued, but not of cued, targets. Thus, our findings implicate gamma coherence in attentional reorienting, linking prefrontal nodes of the VAN and DAN.

This result is in line with the proposal that top-down attention operates using inter/intra-areal cross-frequency coupling (Esghaei et al., 2022). We show that gamma synchronization among right-lateralized frontal regions facilitates attentional redistribution. Communication-through-coherence (Fries, 2015) may enable this information transfer, supported by short-range U-shaped tracts linking the superior and middle frontal gyri (Catani et al., 2012). We establish a clear anatomo-functional relationship for gamma oscillations associated with attentional mechanisms in the prefrontal cortex (Fernández et al., 2023; Veniero et al., 2021), and we reveal a novel pattern of communication within frontal lobe regions. Gamma synchronization may reflect dynamic interactions between the superior longitudinal fasciculus (SLF I-II) pathways facilitating top-down attentional engagement during target anticipation. These connections likely underlie local coordination within the DAN-VAN, integrating spatial cues, sustained attention, and preparatory mechanisms for attentional shifts, potentially via SLF I–II pathways.

Limitations of the present study

Our ROI-based approach enabled targeted analyses of frontoparietal networks but may have overlooked broader whole-brain activity, limiting the detection of unanticipated neural dynamics. Whole-brain analyses could reveal additional networks involved in attentional reorienting and conscious perception, such as subcortical areas. Additionally, our focus on gamma-band activity, which is important for local and long-range neural communication, excludes potential contributions from other frequency bands previously linked to top-down control and inhibition (Asanowicz et al., 2023; Landry et al., 2024; Meehan et al., 2021). Future work incorporating multiple frequency bands may offer a more comprehensive understanding of attentional and perceptual processes

Conclusion and Future Directions

Our results reveal three spectrotemporal dynamics in hemisphere-asymmetric frontoparietal networks preceding conscious reports of near-threshold targets. These results refine theoretical models of conscious perception, supporting the Global Neuronal Workspace Hypothesis (GNWH; Mashour et al., 2020), through right-lateralized gamma coherence and aligning with emerging views of dynamic attentional gradients (Seidel Malkinson et al., 2024). Gamma synchronization appears to integrate predictive spatial cues with top-down attentional processes, shaping the neural basis of conscious perception. Future work should explore the potential extension of these oscillatory mechanisms to mental imagery, where attention shifts to internally generated representations (Liu, et al., 2023; Nobre & Van Ede, 2023; Spagna et al., 2021, 2024).

Reference List

Asanowicz, D., Panek, B., Kotlewska, I., & Van Der Lubbe, R. (2023). On the Relevance of Posterior and Midfrontal Theta Activity for Visuospatial Attention. *Journal of Cognitive Neuroscience*, *35*(12), 1972–2001. https://doi.org/10.1162/jocn_a_02060

Baillet, S., Mosher, J. C., & Leahy, R. M. (2001). Electromagnetic brain mapping. *IEEE Signal Processing Magazine*, *18*(6), 14–30. https://doi.org/10.1109/79.962275

Bang, J. W., & Rahnev, D. (2017). Stimulus expectation alters decision criterion but not sensory signal in perceptual decision making. *Scientific Reports*, *7*(1), 17072. https://doi.org/10.1038/s41598-017-16885-2

Bartolomeo, P., Liu, J., & Seidel Malkinson, T. (2025). Frontoparietal asymmetries leading to conscious perception. *Trends in Cognitive Sciences*, *29*(3), 222–225. https://doi.org/10.1016/j.tics.2024.12.002

Bartolomeo, P., Thiebaut De Schotten, M., & Chica, A. B. (2012). Brain networks of visuospatial attention and their disruption in visual neglect. *Frontiers in Human Neuroscience*, *6*. https://doi.org/10.3389/fnhum.2012.00110

Behrmann, M., Geng, J. J., & Shomstein, S. (2004). Parietal cortex and attention. *Current Opinion in Neurobiology*, *14*(2), 212–217. https://doi.org/10.1016/j.conb.2004.03.012

Botta, F., Lupiáñez, J., & Chica, A. B. (2014). When endogenous spatial attention improves conscious perception: Effects of alerting and bottom-up activation. *Consciousness and Cognition*, *23*, 63–73. https://doi.org/10.1016/j.concog.2013.12.003

Brookes, M. J., Hale, J. R., Zumer, J. M., Stevenson, C. M., Francis, S. T., Barnes, G. R., Owen, J. P., Morris, P. G., & Nagarajan, S. S. (2011). Measuring functional connectivity using MEG: Methodology and comparison with fcMRI. *NeuroImage*, *56*(3), 1082–1104.

https://doi.org/10.1016/j.neuroimage.2011.02.054

Canolty, R. T., & Knight, R. T. (2010). The functional role of cross-frequency coupling. *Trends in Cognitive Sciences*, *14*(11), 506–515. https://doi.org/10.1016/j.tics.2010.09.001

Carrasco, M. (2011). Visual attention: The past 25 years. *Vision Research*, *51*(13), 1484–1525. https://doi.org/10.1016/j.visres.2011.04.012

Carrasco, M., & Barbot, A. (2019). Spatial attention alters visual appearance. *Current Opinion in Psychology*, *29*, 56–64. https://doi.org/10.1016/j.copsyc.2018.10.010

Chica, A. B., Bartolomeo, P., & Lupiáñez, J. (2013). Two cognitive and neural systems for endogenous and exogenous spatial attention. *Behavioural Brain Research*, *237*, 107–123. https://doi.org/10.1016/j.bbr.2012.09.027

Chica, A. B., Lasaponara, S., Chanes, L., Valero-Cabré, A., Doricchi, F., Lupiáñez, J., & Bartolomeo, P. (2011). Spatial attention and conscious perception: The role of endogenous and exogenous orienting. *Attention, Perception, & Psychophysics*, *73*(4), 1065–1081. https://doi.org/10.3758/s13414-010-0082-6

Chica, A. B., Lasaponara, S., Lupiáñez, J., Doricchi, F., & Bartolomeo, P. (2010). Exogenous attention can capture perceptual consciousness: ERP and behavioural evidence. *NeuroImage*, *51*(3), 1205–1212. https://doi.org/10.1016/j.neuroimage.2010.03.002

Corbetta, M., Kincade, J. M., & Shulman, G. L. (2002). Neural Systems for Visual Orienting and Their Relationships to Spatial Working Memory. *Journal of Cognitive Neuroscience*, *14*(3), 508–523. https://doi.org/10.1162/089892902317362029

Corbetta, M., Patel, G., & Shulman, G. L. (2008). The Reorienting System of the Human Brain: From Environment to Theory of Mind. *Neuron*, *58*(3), 306–324. https://doi.org/10.1016/j.neuron.2008.04.017

De Schotten, M. T., Urbanski, M., Duffau, H., Volle, E., Lévy, R., Dubois, B., & Bartolomeo, P. (2005). Direct Evidence for a Parietal-Frontal Pathway Subserving Spatial Awareness in Humans. *Science*, *309*(5744), 2226–2228. https://doi.org/10.1126/science.1116251

Denison, R. N., Yuval-Greenberg, S., & Carrasco, M. (2019). Directing Voluntary Temporal Attention Increases Fixational Stability. *The Journal of Neuroscience*, *39*(2), 353–363. https://doi.org/10.1523/JNEUROSCI.1926-18.2018

Doricchi, F., Macci, E., Silvetti, M., & Macaluso, E. (2010). Neural Correlates of the Spatial and Expectancy Components of Endogenous and Stimulus-Driven Orienting of Attention in the Posner Task. *Cerebral Cortex*, *20*(7), 1574–1585. https://doi.org/10.1093/cercor/bhp215

Doricchi, F., Thiebautdeschotten, M., Tomaiuolo, F., & Bartolomeo, P. (2008). White matter (dis)connections and gray matter (dys)functions in visual neglect: Gaining insights into the brain networks of spatial awareness. *Cortex*, *44*(8), 983–995. https://doi.org/10.1016/j.cortex.2008.03.006

Dugué, L., Merriam, E. P., Heeger, D. J., & Carrasco, M. (2020). Differential impact of endogenous and exogenous attention on activity in human visual cortex. *Scientific Reports*, *10*(1), 21274. https://doi.org/10.1038/s41598-020-78172-x

Esghaei, M., Treue, S., & Vidyasagar, T. R. (2022). Dynamic coupling of oscillatory neural activity and its roles in visual attention. *Trends in Neurosciences*, *45*(4), 323–335. https://doi.org/10.1016/j.tins.2022.01.003

Fernández, A., Denison, R. N., & Carrasco, M. (2019). Temporal attention improves perception similarly at foveal and parafoveal locations. *Journal of Vision*, *19*(1), 12. https://doi.org/10.1167/19.1.12

Fiebelkorn, I. C., Pinsk, M. A., & Kastner, S. (2018). A Dynamic Interplay within the Frontoparietal Network Underlies Rhythmic Spatial Attention. *Neuron*, *99*(4), 842-853.e8. https://doi.org/10.1016/j.neuron.2018.07.038

Fischl, B. (2012). FreeSurfer. *NeuroImage*, *62*(2), 774–781. https://doi.org/10.1016/j.neuroimage.2012.01.021

Fox, M. D., Corbetta, M., Snyder, A. Z., Vincent, J. L., & Raichle, M. E. (2006). Spontaneous neuronal activity distinguishes human dorsal and ventral attention systems. *Proceedings of the National Academy of Sciences*, *103*(26), 10046–10051. https://doi.org/10.1073/pnas.0604187103

Fries, P. (2023). Rhythmic attentional scanning. *Neuron*, *111*(7), 954–970. https://doi.org/10.1016/j.neuron.2023.02.015

Geng, J. J., Leber, A. B., & Shomstein, S. (2019). Attention and Perception: 40 reviews, 40 views. *Current Opinion in Psychology*, *29*, v–viii. https://doi.org/10.1016/j.copsyc.2019.09.001

Hanning, N. M., Deubel, H., & Szinte, M. (2019). Sensitivity measures of visuospatial attention. *Journal of Vision*, *19*(12), 17. https://doi.org/10.1167/19.12.17

He, X., Humphreys, G., Fan, S., Chen, L., & Han, S. (2008). Differentiating spatial and object-based effects on attention: An event-related brain potential study with peripheral cueing. *Brain Research*, *1245*, 116–125. https://doi.org/10.1016/j.brainres.2008.09.092

Helfrich, R. F., Fiebelkorn, I. C., Szczepanski, S. M., Lin, J. J., Parvizi, J., Knight, R. T., & Kastner, S. (2018). Neural Mechanisms of Sustained Attention Are Rhythmic. *Neuron*, *99*(4), 854-865.e5. https://doi.org/10.1016/j.neuron.2018.07.032

Kaufmann, B. C., Pastore-Wapp, M., Bartolomeo, P., Geiser, N., Nyffeler, T., & Cazzoli, D.

(2024). Severity-Dependent Interhemispheric White Matter Connectivity Predicts Poststroke Neglect Recovery. *The Journal of Neuroscience*, *44*(21), e1311232024. https://doi.org/10.1523/JNEUROSCI.1311-23.2024

Landry, M., Da Silva Castanheira, J., Raz, A., Baillet, S., & Sackur, J. (2024). A lateralized alpha-band marker of the interference of exogenous attention over endogenous attention. *Cerebral Cortex*, *34*(1), bhad457. https://doi.org/10.1093/cercor/bhad457

Liu, J., Bayle, D. J., Spagna, A., Sitt, J. D., Bourgeois, A., Lehongre, K., Fernandez-Vidal, S., Adam, C., Lambrecq, V., Navarro, V., Seidel Malkinson, T., & Bartolomeo, P. (2023). Fronto-parietal networks shape human conscious report through attention gain and reorienting. *Communications Biology*, *6*(1), 730. https://doi.org/10.1038/s42003-023-05108-2

Lunven, M., & Bartolomeo, P. (2017). Attention and spatial cognition: Neural and anatomical substrates of visual neglect. *Annals of Physical and Rehabilitation Medicine*, *60*(3), 124–129. https://doi.org/10.1016/j.rehab.2016.01.004

MacLean, M. W., Hadid, V., Spreng, R. N., & Lepore, F. (2023). Revealing robust neural correlates of conscious and unconscious visual processing: Activation likelihood estimation meta-analyses. *NeuroImage*, *273*, 120088. https://doi.org/10.1016/j.neuroimage.2023.120088

Martín-Signes, M., Chica, A. B., Bartolomeo, P., & Thiebaut De Schotten, M. (2024). Streams of conscious visual experience. *Communications Biology*, *7*(1), 908. https://doi.org/10.1038/s42003-024-06593-9

Mashour, G. A., Roelfsema, P., Changeux, J.-P., & Dehaene, S. (2020). Conscious Processing and the Global Neuronal Workspace Hypothesis. *Neuron*, *105*(5), 776–798.

https://doi.org/10.1016/j.neuron.2020.01.026

Melloni, L., Consortium, C., Ferrante, O., Gorska-Klimowska, U., Henin, S., Hirschhorn, R., Khalaf, A., Lepauvre, A., Liu, L., Richter, D., Vidal, Y., Bonacchi, N., Brown, T., Sri, P., Armendariz, M., Bendtz, K., Ghafari, T., Hetenyi, D., Jeschke, J., … Mudrik, L. (2023). *An adversarial collaboration to critically evaluate theories of consciousness*. https://doi.org/10.21203/rs.3.rs-3101836/v1

Melloni, L., Molina, C., Pena, M., Torres, D., Singer, W., & Rodriguez, E. (2007). Synchronization of Neural Activity across Cortical Areas Correlates with Conscious Perception. *The Journal of Neuroscience*, *27*(11), 2858–2865. https://doi.org/10.1523/JNEUROSCI.4623-06.2007

Mengotti, P., Käsbauer, A.-S., Fink, G. R., & Vossel, S. (2020). Lateralization, functional specialization, and dysfunction of attentional networks. *Cortex*, *132*, 206–222. https://doi.org/10.1016/j.cortex.2020.08.022

Nobre, A. C., & Van Ede, F. (2023). Attention in flux. *Neuron*, *111*(7), 971–986. https://doi.org/10.1016/j.neuron.2023.02.032

Oostenveld, R., Fries, P., Maris, E., & Schoffelen, J.-M. (2011). FieldTrip: Open Source Software for Advanced Analysis of MEG, EEG, and Invasive Electrophysiological Data. *Computational Intelligence and Neuroscience*, *2011*, 1–9. https://doi.org/10.1155/2011/156869

Pollack, I., & Norman, D. A. (1964). A non-parametric analysis of recognition experiments. *Psychonomic Science*, *1*(1–12), 125–126. https://doi.org/10.3758/BF03342823

Portin, K., Vanni, S., Virsu, V., & Hari, R. (1999). Stronger occipital cortical activation to lower than upper visual field stimuli. *Experimental Brain Research*, *124*(3), 287–294.

https://doi.org/10.1007/s002210050625

Rojkova, K., Volle, E., Urbanski, M., Humbert, F., Dell'Acqua, F., & Thiebaut De Schotten, M. (2016). Atlasing the frontal lobe connections and their variability due to age and education: A spherical deconvolution tractography study. *Brain Structure and Function*, *221*(3), 1751–1766. https://doi.org/10.1007/s00429-015-1001-3

Sani, I., Stemmann, H., Caron, B., Bullock, D., Stemmler, T., Fahle, M., Pestilli, F., & Freiwald, W. A. (2021). The human endogenous attentional control network includes a ventro-temporal cortical node. *Nature Communications*, *12*(1), 360. https://doi.org/10.1038/s41467-020-20583-5

Shomstein, S. (2012). Cognitive functions of the posterior parietal cortex: Top-down and bottom-up attentional control. *Frontiers in Integrative Neuroscience*, *6*. https://doi.org/10.3389/fnint.2012.00038

Shomstein, S., & Gottlieb, J. (2016). Spatial and non-spatial aspects of visual attention: Interactive cognitive mechanisms and neural underpinnings. *Neuropsychologia*, *92*, 9–19. https://doi.org/10.1016/j.neuropsychologia.2016.05.021

Shulman, G. L., Pope, D. L. W., Astafiev, S. V., McAvoy, M. P., Snyder, A. Z., & Corbetta, M. (2010). Right Hemisphere Dominance during Spatial Selective Attention and Target Detection Occurs Outside the Dorsal Frontoparietal Network. *The Journal of Neuroscience*, *30*(10), 3640–3651. https://doi.org/10.1523/JNEUROSCI.4085-09.2010

Spadone, S., Betti, V., Sestieri, C., Pizzella, V., Corbetta, M., & Della Penna, S. (2021). Spectral signature of attentional reorienting in the human brain. *NeuroImage*, *244*, 118616. https://doi.org/10.1016/j.neuroimage.2021.118616

Spagna, A., Bayle, D. J., Romeo, Z., Seidel-Malkinson, T., Liu, J., Yahia-Cherif, L., Chica, A.

B., & Bartolomeo, P. (2022). *The cost of attentional reorienting on conscious visual perception: An MEG study* (p. 2020.12.05.413161). bioRxiv. https://doi.org/10.1101/2020.12.05.413161

Szczepanski, S. M., Crone, N. E., Kuperman, R. A., Auguste, K. I., Parvizi, J., & Knight, R. T. (2014). Dynamic Changes in Phase-Amplitude Coupling Facilitate Spatial Attention Control in Fronto-Parietal Cortex. *PLoS Biology*, *12*(8), e1001936. https://doi.org/10.1371/journal.pbio.1001936

Tadel, F., Baillet, S., Mosher, J. C., Pantazis, D., & Leahy, R. M. (2011). Brainstorm: A User-Friendly Application for MEG/EEG Analysis. *Computational Intelligence and Neuroscience*, *2011*, 1–13. https://doi.org/10.1155/2011/879716

Tadel, F., Bock, E., Niso, G., Mosher, J. C., Cousineau, M., Pantazis, D., Leahy, R. M., & Baillet, S. (2019). MEG/EEG Group Analysis With Brainstorm. *Frontiers in Neuroscience*, *13*, 76. https://doi.org/10.3389/fnins.2019.00076

Taulu, S., & Simola, J. (2006). Spatiotemporal signal space separation method for rejecting nearby interference in MEG measurements. *Physics in Medicine and Biology*, *51*(7), 1759–1768. https://doi.org/10.1088/0031-9155/51/7/008

Thiebaut De Schotten, M., Dell' Acqua, F., Forkel, S. J., Simmons, A., Vergani, F., Murphy, D., & Catani, M. (2011). A lateralized brain network for visuospatial attention. *Nature Neuroscience*, *14*(10), 1245–1246. https://doi.org/10.1038/nn.2905

Thiebaut De Schotten, M., Tomaiuolo, F., Aiello, M., Merola, S., Silvetti, M., Lecce, F., Bartolomeo, P., & Doricchi, F. (2014). Damage to White Matter Pathways in Subacute and Chronic Spatial Neglect: A Group Study and 2 Single-Case Studies with Complete Virtual "In Vivo" Tractography Dissection. *Cerebral Cortex*, *24*(3), 691–706.

https://doi.org/10.1093/cercor/bhs351

Toba, M. N., Malkinson, T. S., Howells, H., Mackie, M.-A., & Spagna, A. (2023). Same, Same but Different? A Multi-Method Review of the Processes Underlying Executive Control. *Neuropsychology Review*. https://doi.org/10.1007/s11065-023-09577-4

Tosoni, A., Capotosto, P., Baldassarre, A., Spadone, S., & Sestieri, C. (2023). Neuroimaging evidence supporting a dual-network architecture for the control of visuospatial attention in the human brain: A mini review. *Frontiers in Human Neuroscience*, *17*, 1250096. https://doi.org/10.3389/fnhum.2023.1250096

Urbanski, M., Thiebaut De Schotten, M., Rodrigo, S., Oppenheim, C., Touzé, E., Méder, J.-F., Moreau, K., Loeper-Jeny, C., Dubois, B., & Bartolomeo, P. (2011). DTI-MR tractography of white matter damage in stroke patients with neglect. *Experimental Brain Research*, *208*(4), 491–505. https://doi.org/10.1007/s00221-010-2496-8

Ursino, M., & Pirazzini, G. (2024). Theta–gamma coupling as a ubiquitous brain mechanism: Implications for memory, attention, dreaming, imagination, and consciousness. *Current Opinion in Behavioral Sciences*, *59*, 101433. https://doi.org/10.1016/j.cobeha.2024.101433

Voytek, B. (2010). Shifts in gamma phase–amplitude coupling frequency from theta to alpha over posterior cortex during visual tasks. *Frontiers in Human Neuroscience*, *4*. https://doi.org/10.3389/fnhum.2010.00191

Xiong, Y., Fries, P., & Bastos, A. M. (2023). Which Rhythms Reflect Bottom-Up and Top-Down Processing? In N. Axmacher (Ed.), *Intracranial EEG* (pp. 389–414). Springer International Publishing. https://doi.org/10.1007/978-3-031-20910-9_25

Xuan, B., Mackie, M.-A., Spagna, A., Wu, T., Tian, Y., Hof, P. R., & Fan, J. (2016). The

activation of interactive attentional networks. *NeuroImage*, *129*, 308–319. https://doi.org/10.1016/j.neuroimage.2016.01.017